Acta Crystallographica Section D
Biological Crystallography
ISSN 1399-0047

Mutational and structural study of RipA, a key enzyme in *Mycobacterium tuberculosis* cell division: evidence for the L-to-D inversion of configuration of the catalytic cysteine

Flavia Squeglia,[a]‡ Alessia Ruggiero,[a]‡ Maria Romano,[a,b] Luigi Vitagliano[a] and Rita Berisio[a]*

[a]Institute of Biostructures and Bioimaging, CNR, Naples, Italy, and [b]Dipartimento di Scienze Ambientali, Seconda Università di Napoli, Caserta, Italy

‡ FS and AR contributed equally to this work.

Correspondence e-mail: rita.berisio@unina.it

Received 15 April 2014
Accepted 11 June 2014

PDB references: RipA, C383A mutant, 4q4g; E444A mutant, 4q4t; H432A mutant, 4q4n

RipA is a key cysteine protease of *Mycobacterium tuberculosis* as it is responsible for bacterial daughter-cell separation. Although it is an important target for antimicrobial development, its mechanism of action and its interaction pattern with its substrate are hitherto unknown. By combining crystallographic and mutational studies with functional assays and molecular modelling, it is shown that the catalytic activity of the enzyme relies on a Cys–His–Glu triad and the impact of the mutation of each residue of the triad on the structure and function of RipA is analysed. Unexpectedly, the crystallographic analyses reveal that mutation of the glutamic acid to alanine results in inversion of the configuration of the catalytic cysteine. The consequent burial of the catalytic cysteine side chain explains the enzyme inactivation upon mutation. These data point to a novel role of the acidic residue often present in the triad of cysteine proteases as a supervisor of cysteine configuration through preservation of the local structural integrity.

1. Introduction

An essential process in bacterial growth and division is the synthesis and remodelling of peptidoglycan (PGN), a rigid macropolymer surrounding the cytoplasmic membrane which is critical for providing cell-wall integrity in nearly all bacteria (Meroueh *et al.*, 2006). The remarkable rigidity of PGN allows eubacteria to resist their high intracellular osmotic pressure and confers the specific shape on these microorganisms. PGN is composed of glycan chains of alternating units of GlcNAc (*N*-acetylglucosamine) and MurNAc (*N*-acetylmuramic acid), which are cross-linked by short peptides. In *Mycobacterium tuberculosis* (Mtb), the aetiological agent of tuberculosis, these peptides are L-alanyl-γ-D-glutamyl-*meso*-diaminopimelyl-D-alanine and are linked to the glycan *via* an amide bond between the carboxyl group of MurNAc and the L-Ala amino group of the tetrapeptide (Fig. 1*a*).

Hydrolysis of PGN is associated with cell growth and division as well as resuscitation from dormancy (Squeglia *et al.*, 2011, 2013; Ruggiero *et al.*, 2012, 2013; Correale *et al.*, 2013; Nikitushkin *et al.*, 2013; Martínez-Caballero *et al.*, 2013). A clear correlation exists between the absence of cell-wall hydrolase activity and the failure of bacterial cells to separate (Layec *et al.*, 2009; Hett *et al.*, 2008; Chao *et al.*, 2013). Cell-separating enzymes are usually endowed with endopeptidase domains, such as cysteine histidine aminopeptidase (CHAP) or NlpC/P60 domains, and/or glucosaminidase domains, which hydrolyze the peptide portion of PGN (Layec *et al.*, 2008, 2009; Rossi *et al.*, 2009). A crucial role in the cell division of actively growing Mtb is played by RipA, an endopeptidase belonging to the NlpC/P60 family (Chao *et al.*, 2013; Ruggiero, Marasco *et al.*, 2010). The effect of RipA on bacterial growth is

noteworthy, since deletion of the gene encoding RipA induces a decrease in growth and an abnormal phenotype consisting of branching and chaining bacteria (Hett & Rubin, 2008). This feature makes RipA an excellent candidate as a drug target against tuberculosis. In a previous study, we determined the crystal structure of a self-inactivated form of RipA in which the catalytic site cleft of the enzyme is physically locked by a pro-domain, and proposed that the activation of the RipA zymogen occurs through proteolytic cleavage (Ruggiero, Marasco *et al.*, 2010). Recent work has confirmed that RipA is proteolytically activated *in vivo* and that overproduction of activated RipA produces severe growth defects in Mtb (Chao *et al.*, 2013). Despite the important role of RipA in cell division, nothing is hitherto known on its mechanism of action or on the specificity of the enzyme towards peptidoglycan. This work is intended to explore the structural determinants of the functional activity of RipA, with special attention to identification of the structural requirements for enzyme activation.

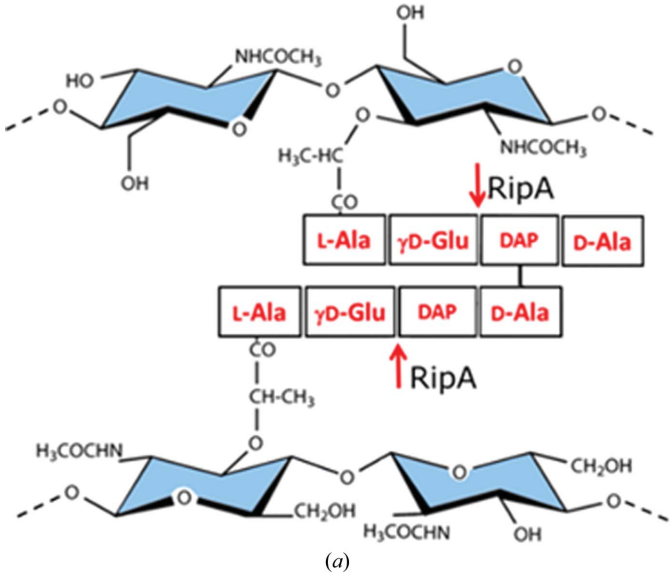

(*a*)

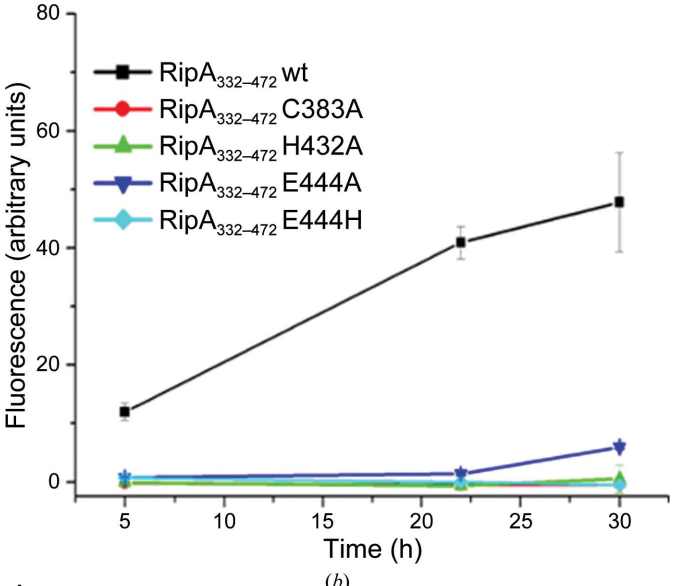

(*b*)

Figure 1
(*a*) Chemical structure of the peptidoglycan of Mtb. Cleavage sites by RipA are shown by arrows. (*b*) FITC-based fluorescence experiments showing the functional activity of RipA variants.

2. Experimental procedures

2.1. Cloning, expression and purification

PCR reactions were carried out to amplify the encoding sequences using *M. tuberculosis* strain H37Rv as a template and forward oligonucleotides starting at Trp263 and Gly332, respectively. *Nco*I/*Hin*dIII-digested fragments were cloned into the pETM-30 and pETM-20 vectors for the expression of $RipA_{263–472}$ and $RipA_{332–472}$, respectively. $RipA_{332–472}$ and its mutants were expressed as N-terminal fusion proteins in *Escherichia coli* BL21 Star (DE3) cells. They were purified by two consecutive rounds of Ni^{2+}-affinity chromatography and gel filtration (Superdex 75 16/60) and concentrated in Vivaspin concentrators [50 m*M* Tris–HCl, 150 m*M* NaCl, 5%(*v*/*v*) glycerol pH 8].

2.2. Mutant preparation

The expression vectors encoding the C383A, H432A and E444A mutations (Supplementary Fig. S1*a*[1]) were generated by site-directed mutagenesis of the wild-type plasmids pETM-30-$RipA_{263–472}$ and pETM-20-$RipA_{332–472}$ using the Stratagene QuikChange kit and the following mutagenic primers: C383A mutant, 5′-CCGTCGGCTTCGACGCCTCAGGCCTGGTG-TTG-3′/5′-CAACACCAGGCCTGAGGCGTCGAAGCCGA-CGG-3′; His432A mutant, 5′-CCGAACGGTAGCCAGGC-CGTGACGATCTACCTC-3′/5′-GAGGTAGATCGTCACG-GCCTGGCTACCGTTCGG-3′; E444A mutant, 5′-CAACG-GCCAGATGCTCGCGGCGCCCGACGTCGG-3′/5′-CCGA-CGTCGGGCGCCGCGAGCATCTGGCCGTTG-3′; E444H mutant, 5′-CAACGGCCAGATGCTCCACGCGCCCGAC-GTCGG-3′/5′-CCGACGTCGGGCGCGTGGAGCATCTGG-CCGTTG-3′. DNA sequencing confirmed the mutations in the recombinant plasmid sequence. Expression and purification of mutants were performed using the same conditions as for the unmutated enzymes.

2.3. Circular dichroism

All CD spectra were recorded with a Jasco J-810 spectropolarimeter equipped with a Peltier temperature-control system (Model PTC-423-S). The molar ellipticity per mean residue, $[\theta]$ (deg cm^2 dmol^{-1}), was calculated from the equation $[\theta] = [\theta]_{obs} \times mrw \times (10lC)^{-1}$, where $[\theta]_{obs}$ is the ellipticity measured in degrees, mrw is the mean residue molecular mass (105.3 Da), C is the protein concentration in g l^{-1} and l is the optical path length of the cell in centimetres. Far-UV measurements (183–250 nm) were carried out at 20°C using a 0.1 cm optical path-length cell and a protein concentration of 0.2 mg ml^{-1}.

[1] Supporting information has been deposited in the IUCr electronic archive (Reference: RR5075).

2.4. Crystallization, data collection and processing

Crystallization trials were performed at 293 K using the hanging-drop vapour-diffusion method. The best crystals of the C383A and H432A mutants were obtained in the same conditions as used for the native protein using protein concentrations of 5 and 8 mg ml^{-1}, respectively, with 8%(*v*/*v*) 2-propanol, 16%(*w*/*v*) PEG 4000 in 60 m*M* sodium citrate trihydrate buffer pH 5.6 (Ruggiero, Squeglia *et al.*, 2010). Crystals of the E444A mutant were obtained using a protein concentration of 8 mg ml^{-1} with 2.0 *M* sodium formate in 0.1 *M* sodium acetate trihydrate buffer pH 4.6. Diffraction data were recorded in-house at 100 K using a Rigaku MicroMax-007 HF generator producing Cu *Kα* radiation equipped with a Saturn944 CCD detector, whereas diffraction data for the C383A mutant were collected on beamline BM14 at the ESRF, Grenoble, France (Table 1). Cryoprotection was achieved by fast-soaking in a solution containing glycerol at a final concentration of 30%(*v*/*v*). The data sets were scaled and merged using the *HKL*-2000 program package (Otwinowski & Minor, 1997). Statistics of data collection are reported in Table 1.

2.5. Structure refinement

The crystal structures were refined against the structure of $RipA_{263–472}$. Crystallographic refinement was carried out against 95% of the measured data using the *CCP*4 program suite (Winn *et al.*, 2011). The remaining 5% of the observed data, which was randomly selected, was used in R_{free} calculations to monitor the progress of refinement. The refinement was started with rigid-body refinement, followed by restrained refinement in *REFMAC* (Murshudov *et al.*, 2011). Water molecules were incorporated into the structure in several rounds of successive refinement. In the case of the C383A mutant, the crystals of which diffracted to atomic resolution, CGLS refinement cycles were performed using *SHELXL*-97 (Sheldrick, 2008). Initial rounds of restrained CGLS refinement were carried out by keeping all atomic displacement parameters (ADPs) isotropic. Subsequently, the ADPs were converted to anisotropic values, leading to improved Fourier maps. The bulk solvent was modelled based on Babinet's principle, as implemented in the SWAT option in *SHELXL*. An approximately isotropic behaviour was attributed to solvent atoms (ISOR restraint). The final round of refinement was carried out with the inclusion of riding H atoms for protein residues. The positions of H atoms assigned based on known geometrical criteria were not refined. The structures of the C383A, H432A and E444A mutants were validated using *PROCHECK* (Laskowski *et al.*, 1996) and deposited in the PDB (accession codes 4q4g, 4q4n and 4q4t, respectively.

2.6. Cell-wall degradation assays

PGN from *Bacillus subtilis* (Sigma) was labelled with fluoroscein isothiocyanate (FITC) by covalently linking FITC to amine groups in the cell wall. This reaction was carried out at 20°C for 16 h under protection from light. The reaction was stopped and the mixture was centrifuged; the insoluble material was washed until the supernatant was completely colourless to eliminate unreacted fluorochrome. The labelled insoluble material was resuspended and stored at −20°C in 4× reaction buffer [50 m*M* Tris–HCl, 10 m*M* $MgCl_2$, 2 m*M* $MnCl_2$, 100 m*M* NaH_2PO_4, 50 m*M* KCl, 0.01%(*v*/*v*) CHAPS]. $RipA_{332–472}$ and its mutants were incubated with FITC-labelled cells at 30°C in the reaction buffer; the insoluble substrate was centrifuged (16 000*g*) and soluble FITC conjugates were measured in triplicate with filters for excitation at 492 nm and emission at 518 nm. The buffer alone was used to correct for background release of FITC.

Table 1
Data-collection and refinement statistics.

Values in parentheses are for the outermost shells.

	$RipA_{263–472}$ C383A	$RipA_{263–472}$ H432A	$RipA_{263–472}$ E444A
Data collection			
Space group	$P2_12_12_1$	$P2_12_12_1$	$P2_12_12_1$
Unit-cell parameters (Å)	*a* = 36.76, *b* = 65.51, *c* = 67.98	*a* = 36.70, *b* = 65.49, *c* = 68.33	*a* = 36.71, *b* = 65.27, *c* = 68.20
Resolution range (Å)	30–0.97 (1.00–0.97)	30–1.39 (1.43–1.38)	30–1.63 (1.66–1.63)
No. of unique reflections	97211	32925	20862
Average multiplicity	8.9 (6.4)	5.0 (3.5)	4.7 (2.6)
R_{merge} (%)	5.4 (45.0)	4.8 (9.0)	6.1 (18.0)
Completeness (%)	99.4 (99.9)	98.8 (90.0)	98.5 (77.3)
Mean $I/\sigma(I)$	43.8 (2.9)	61.0 (15.1)	39.0 (6.0)
Refinement			
R/R_{free} (%)	13.4/16.2	12.4/15.8	14.0/19.0
R.m.s. deviations			
Bond lengths (Å)	0.01	0.01	0.01
Bond angles (°)	1.5	1.6	1.7

2.7. Modelling studies and bioinformatics analyses

The conformation of the muropeptide GlcNAc-MurNAc-L-Ala-*γ*-D-Glu-mesoDAP-D-Ala was modelled into the binding cleft of RipA using the structure of the complex between L-Ala-*γ*-D-Glu and endopeptidase YkfC from *B. cereus* as a template (Xu *et al.*, 2010). The resulting model was energy-minimized using *GROMACS* (Lindorff-Larsen *et al.*, 2010). Sequence-conservation studies were carried out using *ConSurf* (Goldenberg *et al.*, 2009). The homologue search algorithm *CSI-BLAST* was used to retrieve sequences from the UniRef90 sequence database (150 sequences). Sequences were aligned using the *MAFFT* L-INS-I alignment method (the minimal and maximal sequence identities were 35 and 95%, respectively).

3. Results and discussion

The catalytic domain of RipA comprises a central *β*-sheet of six antiparallel *β*-strands, a small two-stranded *β*-sheet and six helices arranged in an *αββαααββββββ* topology (Ruggiero, Marasco *et al.*, 2010). Among the residues of the catalytic site cleft, Cys383 and His432 are fully conserved (Supplementary Figs. S1 and S2). Inspection of the local structure of RipA does not reveal the presence of the histidine residue that typically

completes the catalytic triad in most NlpC/P60 domains (Supplementary Fig. S2). To investigate the contribution of these potential catalytic residues to both the structure and the function of RipA, we produced recombinant mutants with alanine in place of either Cys383, His432 or Glu444. Moreover, we also replaced Glu444 with a histidine, with the aim of generating the canonical NlpC/P60 Cys–His–His triad in RipA (Supplementary Fig. S1).

The effects of the mutations on the enzyme activity were tested using its unlocked form ($RipA_{332–472}$), in which the pro-domain (residues 263–331) that blocks the active-site cleft (Ruggiero, Marasco *et al.*, 2010) is removed. CD spectra were recorded for all unlocked variants to exclude an effect of the mutations on the structural integrity of the enzyme (Supplementary Fig. S3). The cell-wall degrading activity of all variants was measured using PGN from *B. subtilis* labelled with FITC. Fluorescence measurements of supernatants at various time intervals clearly showed that the hydrolytic activity of RipA is equally suppressed upon the mutation to alanine of either His432 or Cys383 (Fig. 1*b*). This finding was predictable since the Cys/His catalytic dyad of RipA superposes well with that of papain, thus suggesting a catalytic mechanism which involves the polarization of the thiol group of Cys383 by the imidazole of His432 to form a thiolate that attacks the electrophilic group at the scissile bond (Fig. 1; Kamphuis *et al.*, 1984; Storer & Ménard, 1994).

The mutation to alanine of Glu444 (E444A), the third residue of the putative RipA catalytic triad, leads to a complete inactivation of the enzyme with a complete loss of PGN degradation activity (Fig. 1*b*). This result was unexpected since mutations of the third residue of the triad in proteases are usually not sufficient to suppress enzyme activity (Zhang *et al.*, 2011). Intriguingly, replacement of Glu444 with histidine (E444H) also has dramatic effects on the enzyme functionality, thus demonstrating that the simple Glu/His replacement is not sufficient to generate the canonical NlpC/P60 Cys–His–His catalytic triad in RipA. Together, these findings suggest that a Cys–His–Glu catalytic triad operates in RipA and that a crucial role is played by Glu444.

To shed light on the atomic-level details of the catalytic mechanism of RipA, we performed crystallographic studies of mutants. Since the unlocked form of the enzyme $RipA_{332–472}$

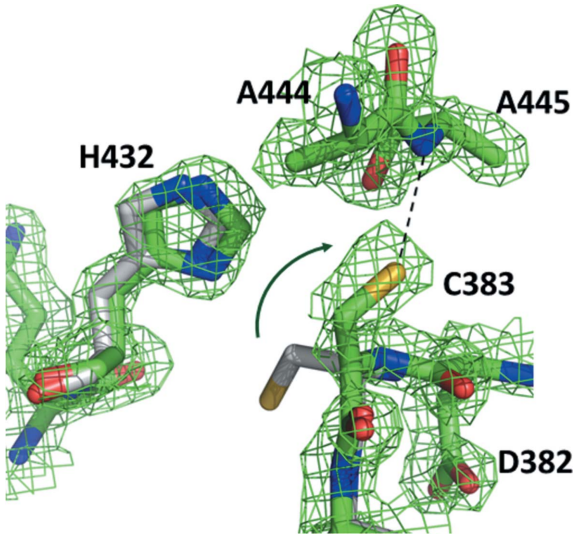

Figure 2
(*a*) OMIT ($2F_o - F_c$) electron-density map of the catalytic site of the E444A mutant. The electron density clearly shows that Cys383 adopts a D-configuration (green). The structure of the wild-type protein, with Cys383 in its canonical L-configuration, is shown in grey.

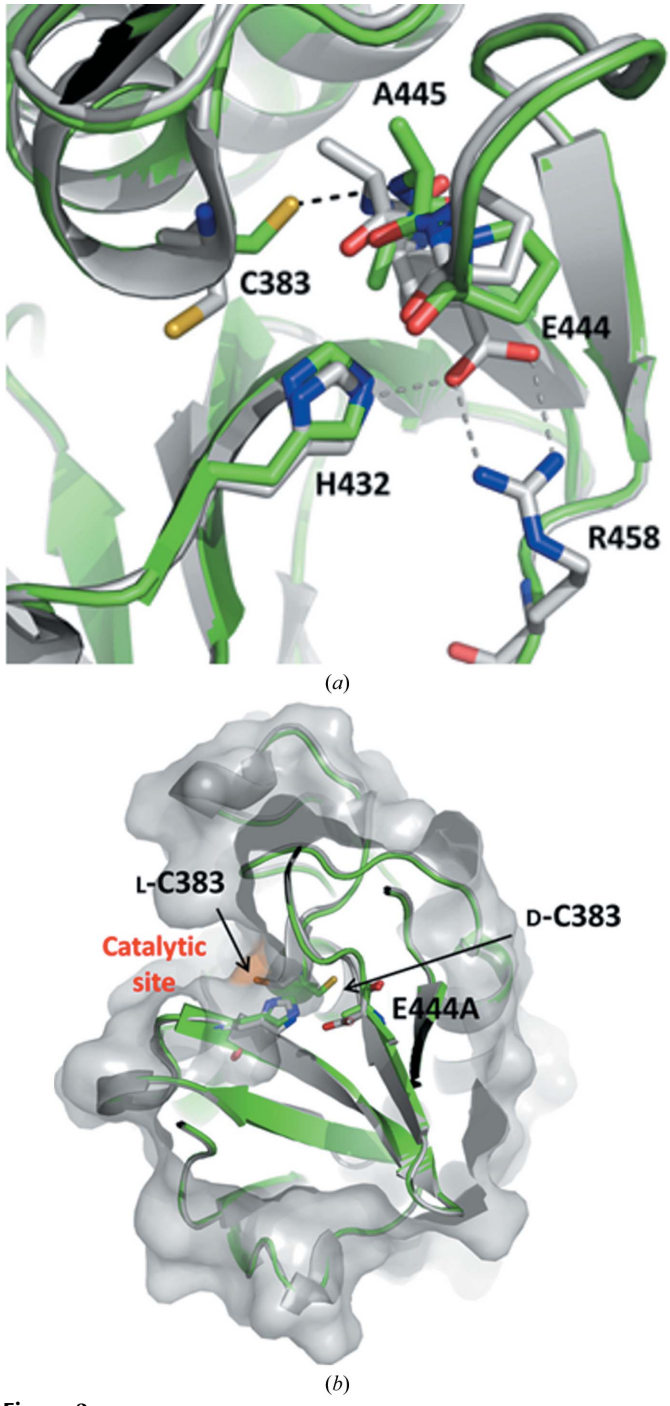

Figure 3
(*a*) Superposition of the catalytic triad in wild-type RipA (grey) and the E444A mutant (green). The hydrogen bonds established by E444A and by wild-type RipA are shown in black and grey, respectively. (*b*) The cartoon and surface representation shows that D-Cys383 is fully buried in the E444A mutant.

was not amenable to crystallization, we crystallized mutants of the locked form of the protein ($RipA_{263–472}$), which includes the pro-domain (Ruggiero, Marasco *et al.*, 2010). In line with a previous independent report (Böth *et al.*, 2011), the structure of the C383A mutant shows minimal perturbation of the RipA active site (Supplementary Fig. S4*a*). Analysis of the active site of the H432A mutant indicates that the cavity created by the replacement of His is filled by water molecules (Supplementary Fig. S4*b*) and that the orientation of the Cys383 side chain is not affected by the mutation of the His432 side chain.

The crystal structure of the E444A mutant was crucial to understanding the structural basis of its inactivity. In contrast to the other mutants, analysis of the catalytic site shows that significant local changes are produced by the E444A mutation (Figs. 2 and 3). Most importantly, the catalytic Cys383 adopts an unprecedented D-configuration (Fig. 2) and its side chain points in the opposite direction to the catalytic site cleft, towards the inner core of the enzyme. Inversions of configuration are unusual in proteins and have been associated with protein destabilization in the degradation pathways of long-lived proteins (Kreil, 1994; Tomiyama *et al.*, 1994; Heck *et al.*, 1994; Buczek *et al.*, 2005). In the crystal structure of the E444A mutant, D-C383 is fully buried and forms a hydrogen-bonding interaction with the backbone N atom of Ala445 and hydrophobic interactions with the side chain of Ala444 (Figs. 2 and 3), thus explaining the inactivity of the E444A mutant (Fig. 1*b*). Compared with the wild-type structure, the backbone atoms of residues embedding the mutation site (residues 443–446) are displaced to accommodate the Cys383 side chain (Fig. 3). This conformational rearrangement associated with the inversion of chirality of Cys383 is not compatible with the local structure of the wild-type enzyme, in which the conformational freedom of the loop embedding Glu444 is restricted by a salt bridge between Glu444 and Arg458 (Fig. 3). This rearrangement also allows the binding of two formate molecules, one in place of the L-Cys383 side chain of the wild-type enzyme and a second one replacing the side chain of Glu444 (Supplementary Fig. S4*c*).

In this view, the conformational flexibility gained upon mutation is necessary to allow the conversion of L-Cys383 to D-Cys383 through a direct α-carbon proton-abstraction/readdition mechanism (Cloos & Christgau, 2002). The accumulation of D-Cys383 is likely to be guided by the favourable interactions mediated by its side chain (Fig. 2). Although the precise mechanism of the inversion of configuration remains to be fully elucidated and we cannot exclude an effect of formate in this reaction, it is likely that the reaction is favoured by the presence of the nearby Asp382, a residue which is essential for substrate binding (see below). The impact of the mutation of Glu444 on the chirality of Cys383 is also able to explain the inactivity of the E444H mutant (Fig. 1*b*). Indeed, a histidine in place of Glu444 is unable to establish the observed salt bridge with Arg458 and thereby to lock the loop 443–446 (Fig. 3*a*). Overall, our data show that RipA strictly operates with a Cys–His–Glu triad and that the structural integrity of the triad is safeguarded by Arg458. It is worth noting that in canonical NlpC/P60 domains, which typically contain Cys–His–His triads, the alteration of the

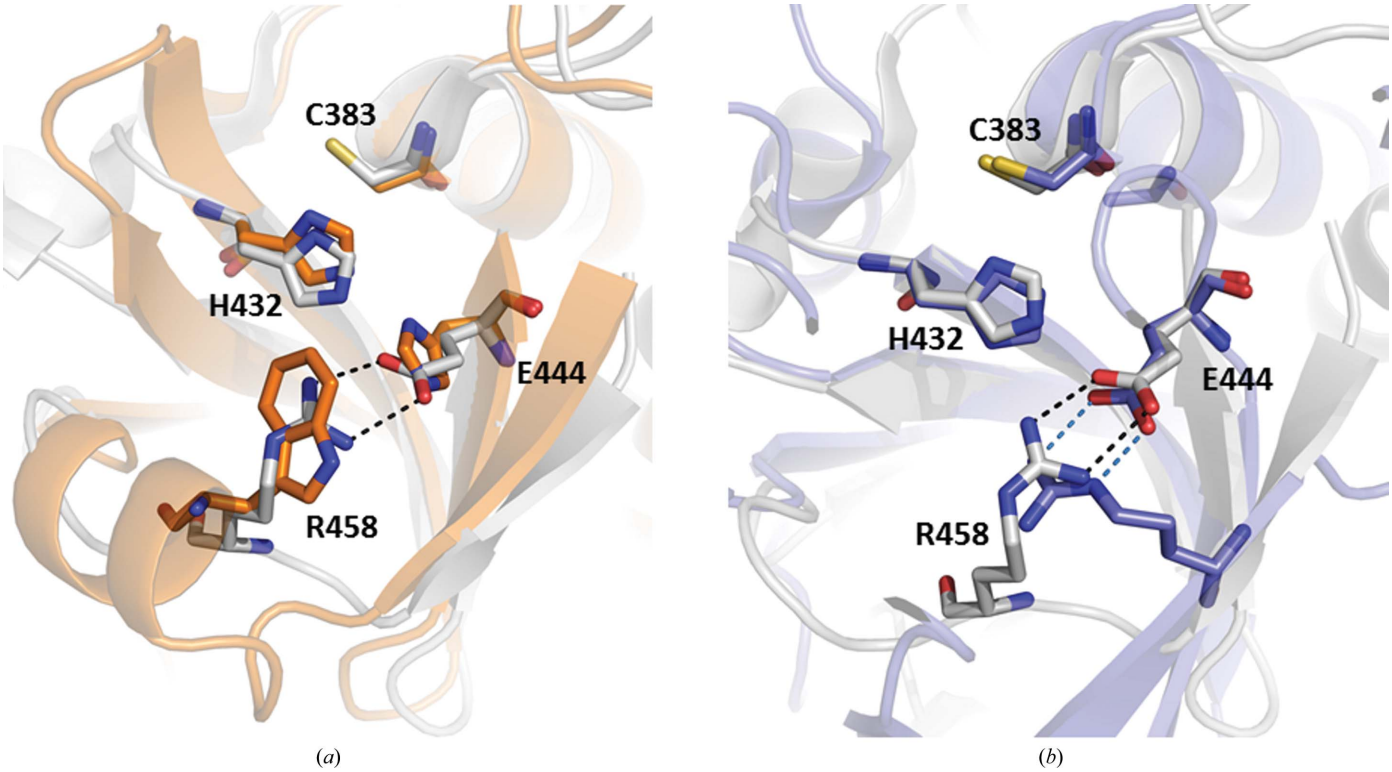

(*a*) (*b*)

Figure 4
Cartoon representation of the RipA catalytic site (grey) after superposition with (*a*) the NlpC/P60 domain of lipoprotein Spr (orange; PDB entry 2k1g) and (*b*) the CHAP domain of glutathionylspermidine synthetase (GSP) from *E. coli* (navy; PDB entry 2io8).

catalytic cysteine is prevented by a higher secondary-structure content of the catalytic site that limits its flexibility (Fig. 4*a*). An architecture of the catalytic triad similar to that of RipA characterizes the more distantly related CHAP domains (sequence identity of up to 11%), which act with either a Cys–His–Glu or a Cys–His–Asp triad. Indeed, the integrity of the triad is also guaranteed in this case by a salt-bridge interaction with an arginine residue (Fig. 4*b*).

We further explored the properties of the RipA active site by studying the recognition mechanism of the enzyme for the muropeptide GlcNAc-MurNAc-L-Ala-γ-D-Glu-mesoDAP-D-Ala. This muropeptide was modelled in the catalytic site cleft, the shape of which accounts well for the branched nature of peptidoglycan. Aside from the catalytic dyad, several residues appear to interact with the muropeptide (Asp382, Ser384, Ser402, Val428, Gln431 and Asp447; Supplementary Fig. S5). Among these, the most conserved is Asp382, which directly contacts γ-D-Glu (Supplementary Figs. S1 and S2); this indicates a strong specificity of RipA towards γ-D-Glu. In contrast, the residues contacting the DAP side chain are characterized by low conservation (*e.g.* Asp447; Supplementary Fig. S1). This finding well agrees with the ability of RipA to hydrolyze both Lys-type (Ruggiero, Marasco *et al.*, 2010) and DAP-type PGN (Fig. 1).

In conclusion, this work provides clear evidence of the inversion of chirality of a catalytic residue, an event which inactivates the enzyme and proves that mutagenesis may have unpredictable consequences on enzyme structures. We show that the structural integrity of the Cys–His–Glu catalytic triad is provided by the acidic residue (Glu444) that is often present in the catalytic triad of cysteine proteases and is currently believed to act solely by aligning and polarizing the basic histidine residue (Zhang *et al.*, 2011). Proteins embedding residues with inverted configuration are considered to be molecular clocks of protein turnover destined for degradation reactions (Amano *et al.*, 2011). Our data show that the inversion of configuration of the catalytic Cys383 to its D-isomer, resulting in full inactivation of RipA, is safeguarded by the acidic residue of the catalytic triad, Glu444 (Figs. 1*b* and 3). In this respect, Glu444 emerges as an unexpected regulator of catalysis which acts by restraining the local flexibility of the catalytic site.

The authors thank the COST Action BM1003 (COST-Grants-BM1003-00772) and the Mizutani Foundation for Glycoscience for financial support.

References

Amano, M., Hasegawa, J., Kobayashi, N., Kishi, N., Nakazawa, T., Uchiyama, S. & Fukui, K. (2011). *Anal. Chem.* **83**, 3857–3864.

Böth, D., Schneider, G. & Schnell, R. (2011). *J. Mol. Biol.* **413**, 247–260.

Buczek, O., Yoshikami, D., Bulaj, G., Jimenez, E. C. & Olivera, B. M. (2005). *J. Biol. Chem.* **280**, 4247–4253.

Chao, M. C., Kieser, K. J., Minami, S., Mavrici, D., Aldridge, B. B., Fortune, S. M., Alber, T. & Rubin, E. J. (2013). *PLoS Pathog.* **9**, e1003197.

Cloos, P. A. & Christgau, S. (2002). *Matrix Biol.* **21**, 39–52.

Correale, S., Ruggiero, A., Capparelli, R., Pedone, E. & Berisio, R. (2013). *Acta Cryst.* D**69**, 1697–1706.

Goldenberg, O., Erez, E., Nimrod, G. & Ben-Tal, N. (2009). *Nucleic Acids Res.* **37**, D323–D327.

Heck, S. D. *et al.* (1994). *Science*, **266**, 1065–1068.

Hett, E. C., Chao, M. C., Deng, L. L. & Rubin, E. J. (2008). *PLoS Pathog.* **4**, e1000001.

Hett, E. C. & Rubin, E. J. (2008). *Microbiol. Mol. Biol. Rev.* **72**, 126–156.

Kamphuis, I. G., Kalk, K. H., Swarte, M. B. & Drenth, J. (1984). *J. Mol. Biol.* **179**, 233–256.

Kreil, G. (1994). *Science*, **266**, 996–997.

Laskowski, R. A., Rullmannn, J. A., MacArthur, M. W., Kaptein, R. & Thornton, J. M. (1996). *J. Biomol. NMR*, **8**, 477–486.

Layec, S., Decaris, B. & Leblond-Bourget, N. (2008). *Res. Microbiol.* **159**, 507–515.

Layec, S., Gérard, J., Legué, V., Chapot-Chartier, M.-P., Courtin, P., Borges, F., Decaris, B. & Leblond-Bourget, N. (2009). *Mol. Microbiol.* **71**, 1205–1217.

Lindorff-Larsen, K., Piana, S., Palmo, K., Maragakis, P., Klepeis, J. L., Dror, R. O. & Shaw, D. E. (2010). *Proteins*, **78**, 1950–1958.

Martínez-Caballero, S., Lee, M., Artola-Recolons, C., Carrasco-López, C., Hesek, D., Spink, E., Lastochkin, E., Zhang, W., Hellman, L. M., Boggess, B., Mobashery, S. & Hermoso, J. A. (2013). *J. Am. Chem. Soc.* **135**, 10318–10321.

Meroueh, S. O., Bencze, K. Z., Hesek, D., Lee, M., Fisher, J. F., Stemmler, T. L. & Mobashery, S. (2006). *Proc. Natl Acad. Sci. USA*, **103**, 4404–4409.

Murshudov, G. N., Skubák, P., Lebedev, A. A., Pannu, N. S., Steiner, R. A., Nicholls, R. A., Winn, M. D., Long, F. & Vagin, A. A. (2011). *Acta Cryst.* D**67**, 355–367.

Nikitushkin, V. D., Demina, G. R., Shleeva, M. O. & Kaprelyants, A. S. (2013). *Antonie Van Leeuwenhoek*, **103**, 37–46.

Otwinowski, Z. & Minor, W. (1997). *Methods Enzymol.* **276**, 307–326.

Rossi, P., Aramini, J. M., Xiao, R., Chen, C. X., Nwosu, C., Owens, L. A., Maglaqui, M., Nair, R., Fischer, M., Acton, T. B., Honig, B., Rost, B. & Montelione, G. T. (2009). *Proteins*, **74**, 515–519.

Ruggiero, A., De Simone, P., Smaldone, G., Squeglia, F. & Berisio, R. (2012). *Curr. Protein Pept. Sci.* **13**, 756–766.

Ruggiero, A., Marasco, D., Squeglia, F., Soldini, S., Pedone, E., Pedone, C. & Berisio, R. (2010). *Structure*, **18**, 1184–1190.

Ruggiero, A., Marchant, J., Squeglia, F., Makarov, V., De Simone, A. & Berisio, R. (2013). *J. Biomol. Struct. Dyn.* **31**, 195–205.

Ruggiero, A., Squeglia, F., Esposito, C., Marasco, D., Pedone, E., Pedone, C. & Berisio, R. (2010). *Protein Pept. Lett.* **17**, 70–73.

Sheldrick, G. M. (2008). *Acta Cryst.* A**64**, 112–122.

Squeglia, F., Marchetti, R., Ruggiero, A., Lanzetta, R., Marasco, D., Dworkin, J., Petoukhov, M., Molinaro, A., Berisio, R. & Silipo, A. (2011). *J. Am. Chem. Soc.* **133**, 20676–20679.

Squeglia, F., Romano, M., Ruggiero, A., Vitagliano, L., De Simone, A. & Berisio, R. (2013). *Biophys. J.* **104**, 2530–2539.

Storer, A. C. & Ménard, R. (1994). *Methods Enzymol.* **244**, 486–500.

Tomiyama, T., Asano, S., Furiya, Y., Shirasawa, T., Endo, N. & Mori, H. (1994). *J. Biol. Chem.* **269**, 10205–10208.

Winn, M. D. *et al.* (2011). *Acta Cryst.* D**67**, 235–242.

Xu, Q. *et al.* (2010). *Acta Cryst.* F**66**, 1354–1364.

Zhang, W., Sulea, T., Tao, L., Cui, Q., Purisima, E. O., Vongsamphanh, R., Lachance, P., Lytvyn, V., Qi, H., Li, Y. & Ménard, R. (2011). *Biochemistry*, **50**, 4775–4785.